T. Nishioka
Visiting Assistant Professor.

M. Perl
Research Scientist II.

S. N. Atluri
Regents' Professor of Mechanics.

Center for the Advancement
of Computational Mechanics,
School of Civil Engineering,
Georgia Institute of Technology,
Atlanta, Ga. 30332

An Analysis of Dynamic Fracture in an Impact Test Specimen

Numerical simulations of fast fracture in four cases of dynamic tear test experiments on 4340 steel are performed using a moving singular finite element method. The experimentally measured crack propagation histories are used as input data to the so-called generation phase simulations to determine the dynamic stress intensity factor histories. In most numerical analyses of dynamic fracture specimens, the load and support points have been treated as fixed boundary conditions. In the present paper, more realistic boundary conditions (contact/no-contact), in which the specimen can separate from the tup and the supports are introduced. The results are also discussed in the light of current controversies surrounding the dynamic fracture toughness properties governing crack propagation under impact loading.

1 Introduction

Until recently, for situations governed by small-scale yielding, it was thought that the governing criterion for elastodynamic crack propagation under Mode I plane strain conditions can be written as

$$K_I(v,t) = K_{ID}(v)$$

where $K_{ID}(v)$ is the velocity-dependent fracture toughness of the material, which was thought to be a "reasonably geometry-independent" material property. This hypothesis appeared to have been validated in several studies related to dynamic crack-propagation initiated under quasi-static loading.

In the analysis of such cases, both "generation" and 'propagation" calculations were employed. In the former calculation, the experimentally measured crack-propagation history was simulated to find the stress intensity factor or the velocity-dependent fracture toughness. The latter calculation was used in either of the two ways: (*i*) based on a given K_{ID} versus v relation to find the crack propagation history, or (*ii*) to find the best K_{ID} versus v relation, the calculated crack-propagation history corresponding to which agreed best with the experiment. The remarkable success of these calculations appeared to indicate that the prediction of dynamic crack-propagation and possible arrest under general loading conditions may be well within the grasp of current art of computational mechanics.

Recently some work has appeared, however, that seemed to cast doubt on the concept of dynamic fracture toughness that is independent of the rate of applied loading. In reference [1], experimental and numerical results were reported for the dynamic tear test specimens of 4340 steel, a high-strength, rate-insensitive material. In these experiments, crack-propagation was initiated from notches, with varying degree of "bluntness," under impact as well as quasi-static loading. A series of "propagation"-type linear elastodynamic analyses, using hypothetical K_{ID} values, were performed. It was found [1] that the dynamic fracture toughness governing crack-propagation initiated by impact loading may be significantly higher (roughly 170 $MNm^{-1.5}$) than when crack growth is initiated quasi-statically (roughly 65 $MNm^{-1.5}$).

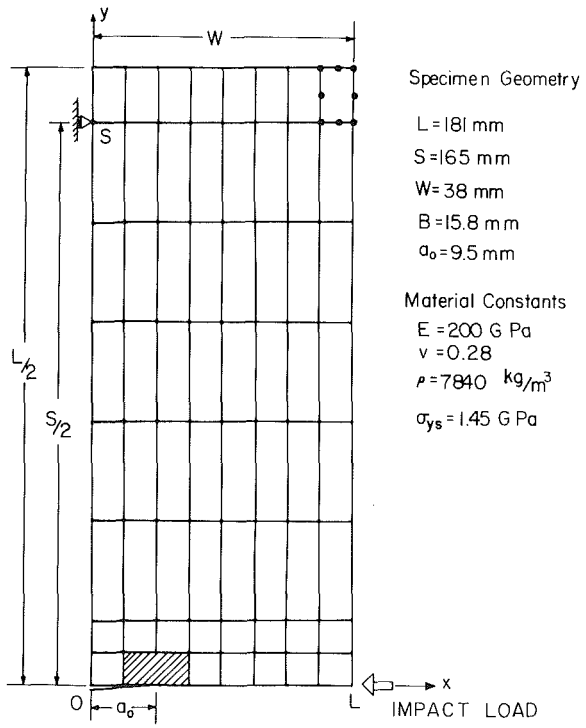

Fig. 1 Finite element mesh for the DTT specimen

Contributed by the Pressure Vessels and Piping Division for publication in the JOURNAL OF PRESSURE VESSEL TECHNOLOGY. Manuscript received by the Pressure Vessels and Piping Division, September 21, 1981; revised manuscript received February 11, 1983.

Table 1 Generation studies

Study no. \ Data	Notch-root diameter	Initiation time	Boundary conditions
DTT 1	0.064 mm	95 μs	Fixed
DTT 2	0.064 mm	95 μs	Contact/ no-contact
DTT 3	0.064 mm	35 μs	Contact/ no-contact
DTT 4	0.000 mm	92.24 μs	Contact/ no-contact

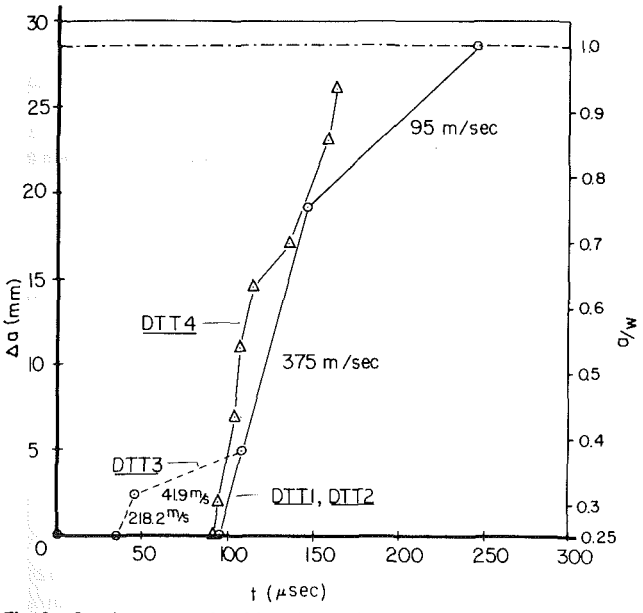

Fig. 2 Crack propagation histories as input data to generation phase fracture simulation

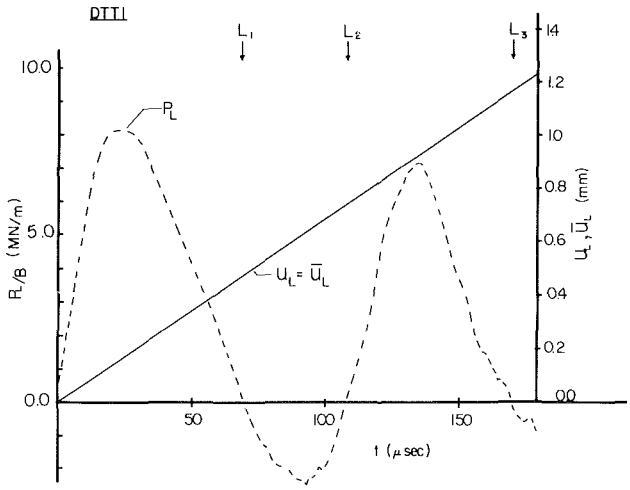

Fig. 3 Variation of tup reaction force and tup displacement (fixed condition)

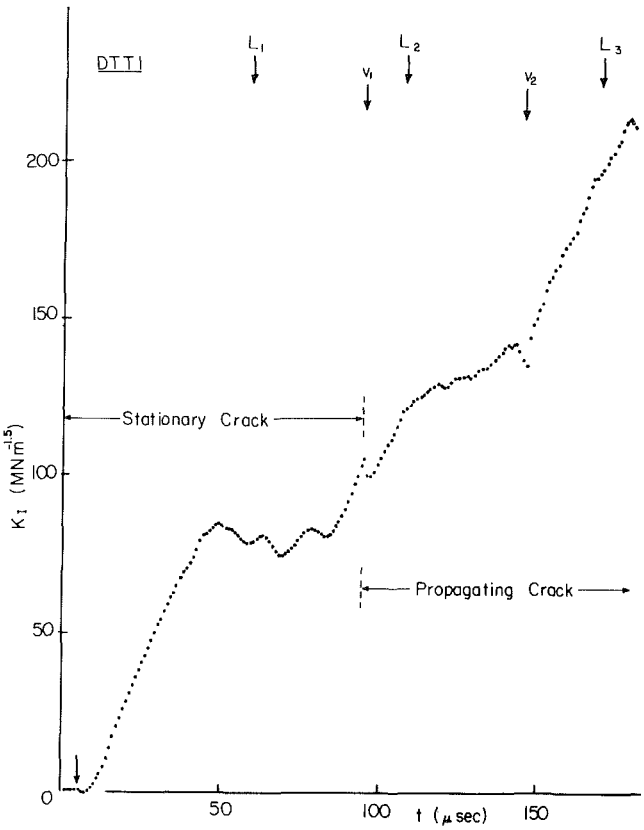

Fig. 4 Variation of dynamic stress intensity factor (DTT1)

The primary objective to the present study is an attempt to analyze the data presented in [1], and to examine the results in the light of the conclusions presented in [1]. In the present paper, "generation"-type analyses were employed in contrast to those in [1]. The employed finite element method is the "moving-singularity" procedure reported earlier by the authors [2, 3], in which the instantaneous stress intensity factor can be determined directly and accurately as one of the parameters in the assumed fields in the singular element. The moving-singularity finite element method has been successfully used in both the generation and the propagation simulations of fast fracture in double-cantilever-beam specimens [4]. In the present analyses, careful attention is paid to the boundary conditions on the specimen, especially the loss of contact of the specimen at various times with either the supports, or the tup, or both. Four different cases of experimental specimen are analyzed. In each case, the variations of input energy, strain energy, kinetic energy, and fracture energy are computed. The balancing of these energy quantities gives an a posteriori check on the accuracy of the present calculations.

Detailed results are presented for each of the four cases analyzed. These results are analyzed to arrive at some "plausible" conclusions which appear to be at variance with the conclusions presented in [1].

2 Analysis

The test specimen geometry is indicated in Fig. 1, along with the finite element mesh employed in the modeled portion of the specimen. Points L and S in Fig. 1 represent, respectively, the loading and support points. Sixty-two 8-noded insoparametric elements and one moving singular element are used. The specimen geometry indicated in Fig. 1 corresponds to that reported in [1], and a plane-strain condition is invoked in the present two-dimensional analysis. In simulating the experiments [1], the following initial conditions are used in the present analysis: at time $t=0$, the tup velocity $\dot{u}_L = 6.88$ m/s. Thus, the tup displacement is calculated by $u_L = \dot{u}_L t$.

In all but one of the present four series of calculations, account is taken of the possibility of lack of contact of the specimen with either the tup or the supports (i.e., the tup and supports can "push" the specimen but not "pull") at various instants of time, as and when the analysis may naturally dictate. In one case, to study the effect of the foregoing

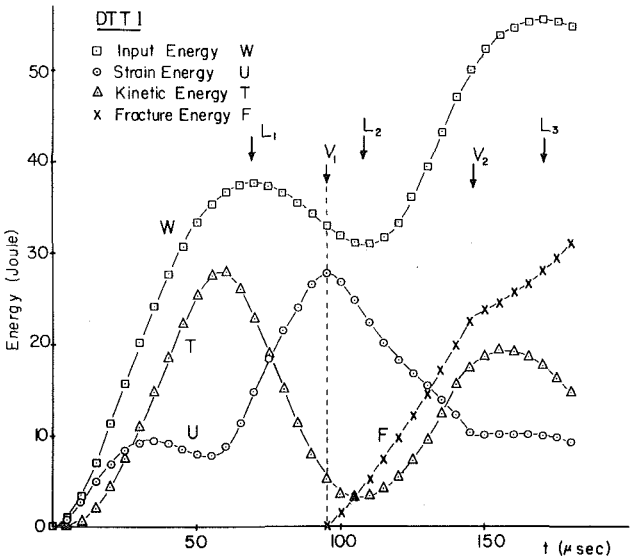

Fig. 5 Energy variations (DTT1)

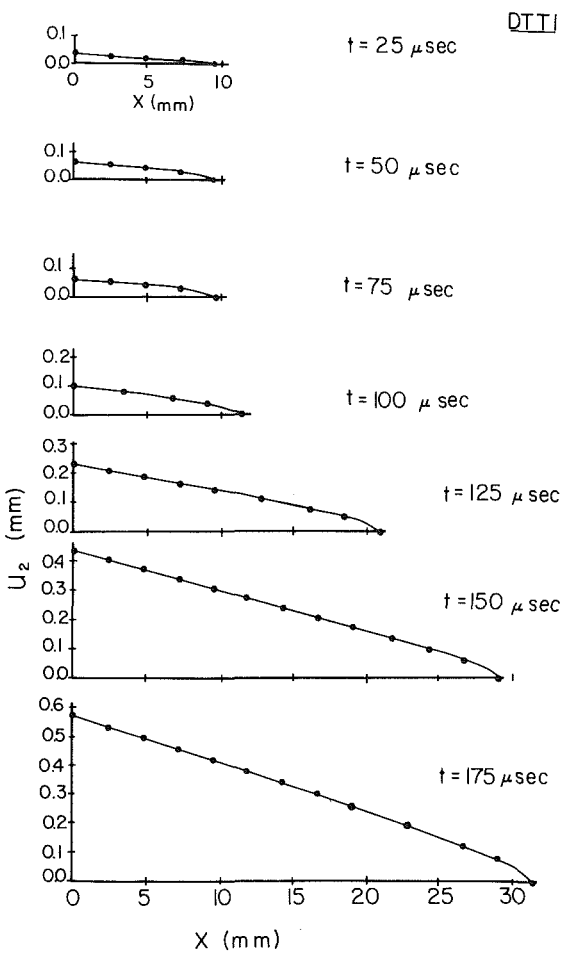

Fig. 6 Crack opening displacements at various times

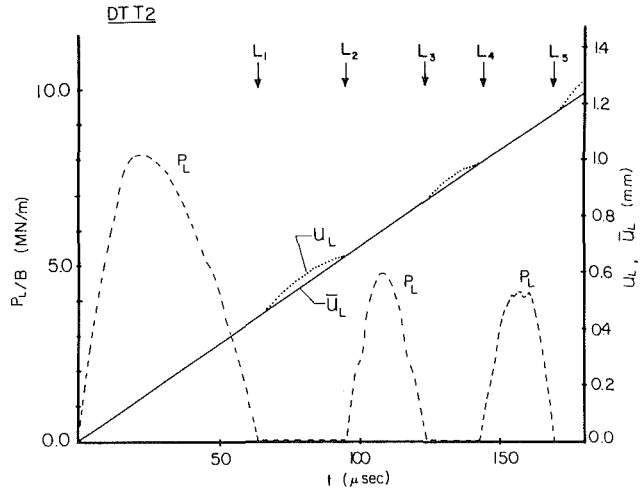

Fig. 7 Variation of tup reaction force and separation of specimen from the tup (DTT2)

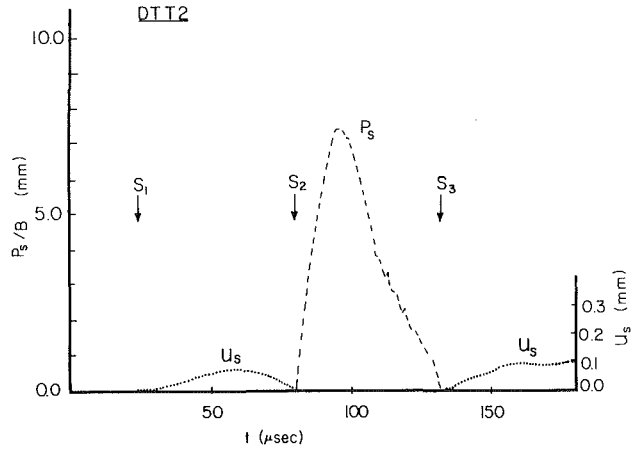

Fig. 8 Variation of support reaction force and separation of specimen from the support (DTT2)

contact/no-contact conditions, the specimen was held "fixed" (i.e., the tup and supports are always in contact with the specimen).

The present series of computations are summarized in Table 1. Also, it is to be understood that the present analyses are the so-called "generation" studies in the sense defined in [1], as opposed to the "propagation" studies performed in [1].

The crack-length versus time histories for the foregoing four cases are shown in Fig. 2. For the cases DTT1 and DTT2, the Δa versus t curves used are the same as that of reference [1], except that the boundary conditions are different as in Table 1. In DTT3 the data point, as shown in Fig. 4 of reference [1], indicates a crack-growth of ~ 2.5 mm at $t \sim 45$ μs was included in the Δa versus t curves, and further, the time of initiation of propagation was chosen such that the K value at initiation was ~ 65 MNm$^{-1.5}$. DTT4 indicates the data obtained for a fatigue pre-cracked specimen [5]; however, the initiation time was determined to be 92.24 μs by extrapolation of the experimental data [5].

Prior to the presentation of the results, we indicate briefly the analysis procedure. As noted earlier, the present analysis of dynamic crack propagation is based on the procedure developed by the authors, and detailed elsewhere [2, 3]. The procedure was also applied to both the generation and the propagation phase fracture simulations [4]. To supplement the mathematical procedure in [2, 3, 4] for the present case, we consider some details of imposing "contact/no-contact" boundary conditions on the specimen.

We designate the force with which either the tup or the supports "push" the specimen as being positive. Using the standard notation, the reaction forces at the points where displacement are prescribed are calculated by

$$\mathbf{P} = \underset{\sim}{\mathbf{K}}\mathbf{q} + \underset{\sim}{\mathbf{m}}\ddot{\mathbf{q}} \tag{1}$$

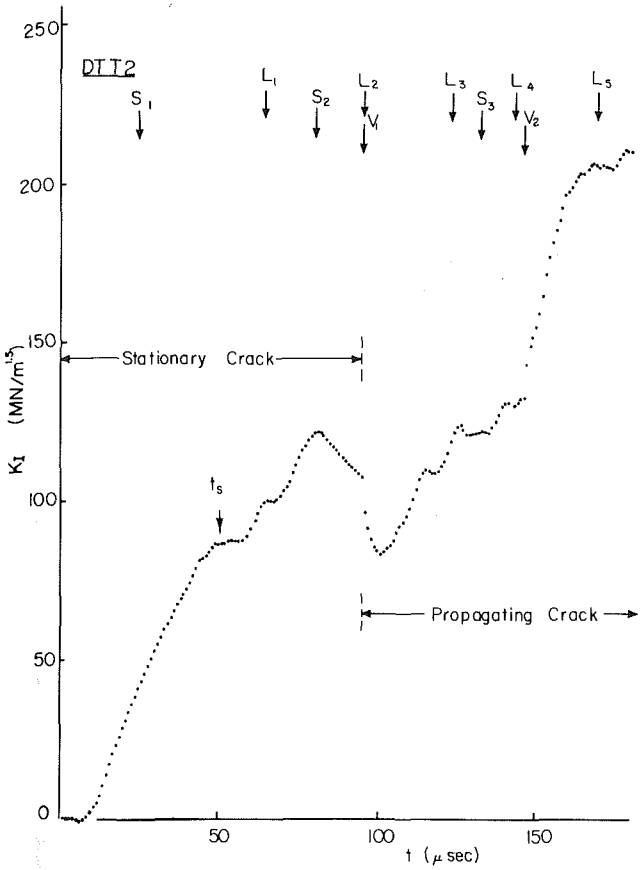

Fig. 9 Variation of dynamic stress intensity factor (DTT2)

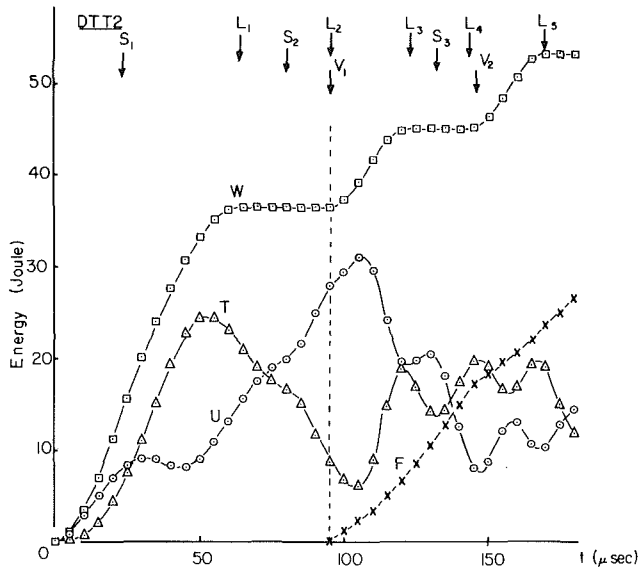

Fig. 10 Energy variations (DTT2)

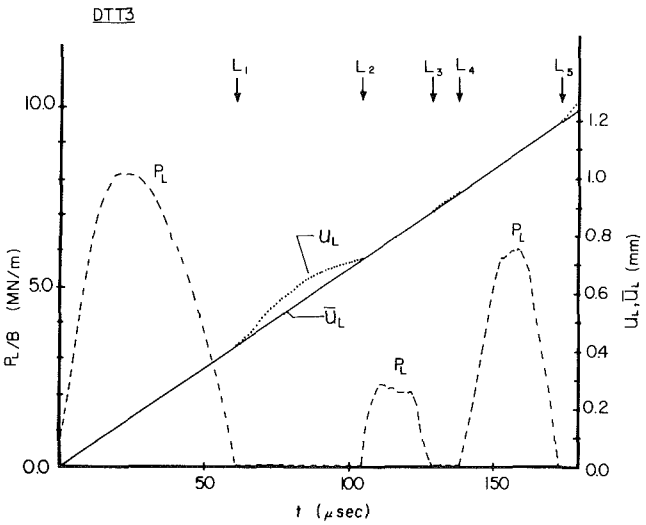

Fig. 11 Variation of tup reaction force and separation of specimen from the tup (DTT3)

The displacement u and reaction force P in the time step $(n+1)$ are predicted by

$$u_{n+1} = u_n + \Delta t_{n+1}\, \dot{u}_n \tag{2}$$

and

$$P_{n+1} = P_n + \frac{(P_n - P_{n-1})}{\Delta t_n}\, \Delta t_{n+1} \tag{3}$$

It is noted that we may use $\Delta t_{n+1} = \Delta t_n = \Delta t$. Assume that P_{n-1} and P_n are positive and that $P_{n-1} > P_n$. The no-contact condition during the time increment (n) to $(n+1)$ is predicted to occur after the subincrement of time

$$\Delta t_c = \frac{P_n}{(P_{n-1} - P_n)}\, \Delta t \tag{4}$$

If $0 \le \Delta t_c \le \Delta t$, during the $(n+1)$ step, we change Δt to Δt_c and perform the analysis with the condition of contact and during $(n+2)$ step, we change Δt to $\Delta t_F (\Delta t_c + \Delta t_F = \Delta t)$, and perform the analysis with the condition of no-contact. This process is repeated.

An analogous scheme is used to predict the transition from a "no-contact" to "contact" condition; however, this time by monitoring the displacements of the respective points of the specimen relative to either the tup or the supports.

Using the procedure described in the foregoing, the influence of the loss of contact of a high-strength steel DCB specimen with the loading wedge has also been investigated in reference [6]. It was found in reference [6] that the effect of separation of the specimen from the loading wedge propagates with a speed of the order of shear wave velocity of the material.

3 Numerical Results for Dynamic Tear Test Specimens

3.1 DTT1 Specimen. In this case, the displacement, velocity, and acceleration at the point L (see Fig. 1) are prescribed. L_1, L_2, and L_3 as shown in Fig. 3 are the times when reaction force at the tup becomes zero (note "positive reaction" implies that the tup is pushing the specimen). Negative "reaction force" is observed during times $L_1 < t < L_2$, and $t > L_3$. The negative force was also observed in the experiment of dynamic tear test [7]. In the experiment, the negative forces were produced by local vibrations of the tup due to the loss of contact with the specimen, while in the DTT1 study, the negative forces were due to the fact that the tup was pulled by the specimen, since the loss of contact is prohibited.

Figure 4 shows the variation of the computed stress intensity factors in the present "generation"-type analysis. The times marked by v_1 and v_2 in Fig. 4 are those when the crack propagates with constant velocities v_1 and v_2, respectively. The apparent initiation fracture toughness for a blunt notch, K_{Qd} obtained in this computation, as seen from Fig. 4 is about 106 MNm$^{-1.5}$.

The computed variation of input, strain, kinetic, and fracture energies with time, are shown in Fig. 5. It is noted that in the present procedures [2, 3] the dynamic K-factors are

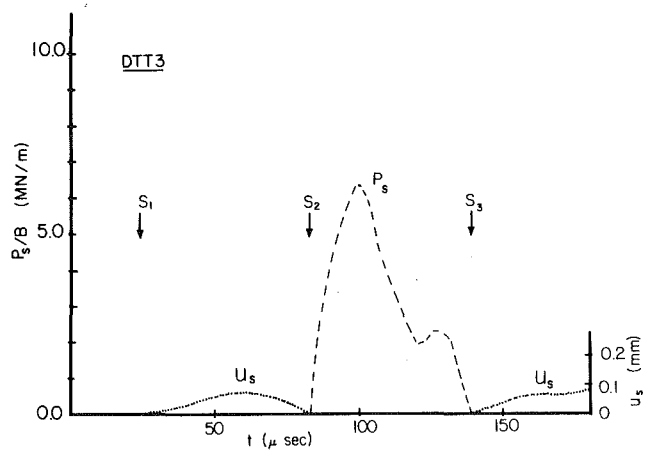

Fig. 12 Variation of support reaction force and separation of specimen from the support (DTT3)

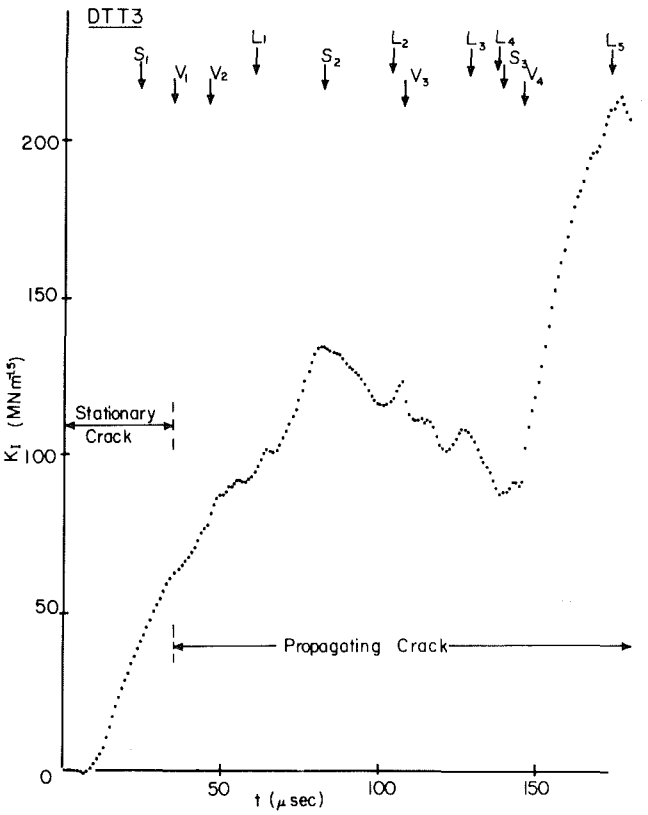

Fig. 13 Variation of dynamic stress intensity factor (DTT3)

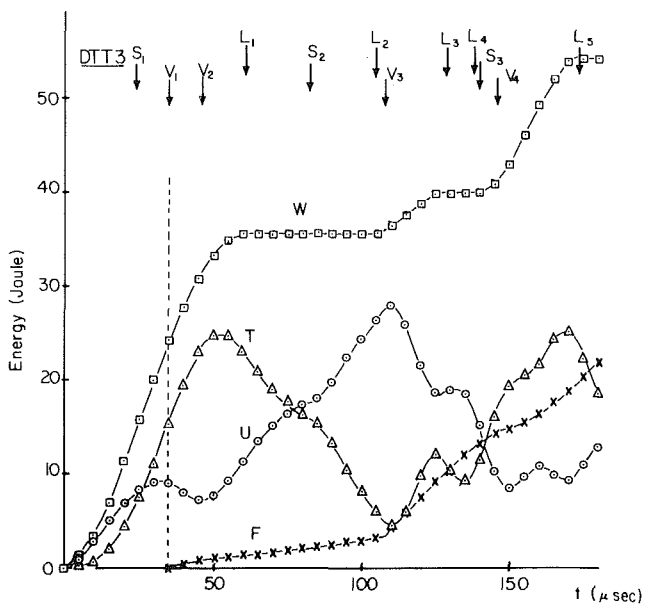

Fig. 14 Energy variations (DTT3)

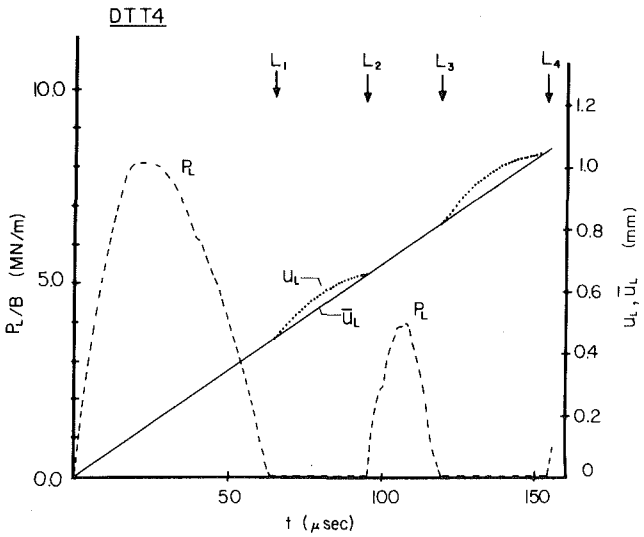

Fig. 15 Variation of tup reaction force and separation of specimen from the tup (DTT4)

solved for directly. From this, the energy release rate is calculated and accumulated as the fracture energy. Alternatively, fracture energy is also calculated directly from a crack-tip integral of work done in separation of crack faces. These two procedures, as discussed in [8], were noted to give almost identical results for the present cases. It is seen from Fig. 5 that during the periods $L_1 < t < L_2$ and $t > L_3$ input energy appears to actually decrease, due to the "negative" reaction forces.

Figure 6 shows the crack profiles at various times. As seen, the profiles are nearly linear except very near the crack tip. From this, a formula has been derived for determining dynamic stress intensity factors directly from crack growth opening displacements [9]. This formula [9] should be of great value in the experimental measurement of dynamic stress-intensity factors for propagating cracks in (opaque) metallic specimens.

3.2 DTT2 Specimen. The condition of contact/no-contact was invoked in this case. As seen from Fig. 7, the specimen is not in contact with the tup during the periods $L_1 < t < L_2$; $L_3 < t < L_4$, and $t > L_5$ as marked. Also, it can be seen from Fig. 8 that the specimen is not in contact with the supports during the times $S_1 < t < S_2$, and $t > S_3$ as marked in Fig. 8. Comparing Figs. 7 and 8, it is seen that the maximum reaction force P_s at the support is very close to the maximum tup load P_L. It is also seen that during the times $L_1 < t < S_2$, $S_3 < t < L_4$ and $t > L_5$, the specimen is not in contact with either the tup or the supports; i.e. the specimen is a free-flying object!

The variation of the computed dynamic K-factor is shown in Fig 9. It is seen that the apparent initiation toughness, K_{Qd}, is again about 108 MNm$^{-1.5}$. However, prior to initiation, K_I value appears to reach 122 MNm$^{-1.5}$ ($> K_{Qd}$) at 82 μs.

In order to investigate the propagation speed of the "no-contact" effect, the time of arrival of the elastic shear wave emanating from the support at $t = S_1$ to the crack tip is indicated as t_s in Fig. 9. Comparing Figs. 4 and 9, it is seen that at $t = t_s$, the stress intensity factor variation in the DTT2

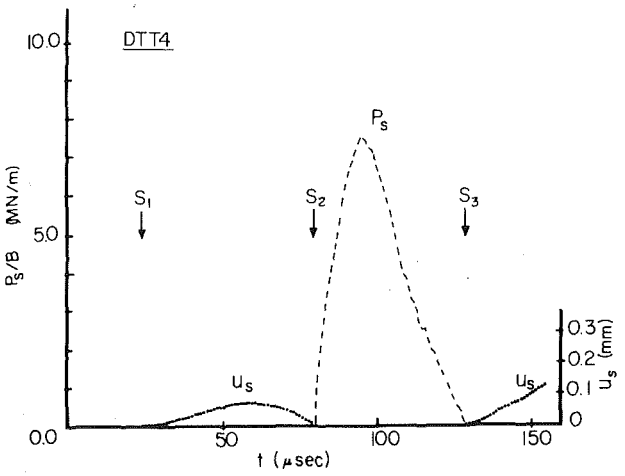

Fig. 16 Variation of support reaction force and separation of specimen from the support (DTT4)

specimen begins to change from that in the DTT1 case. Thus, as found in a DCB specimen [6], in the DTT specimen the no-contact effect also propagates with a speed of the order of shear wave velocity. Higher magnitudes of stress intensity factor in the DTT2 case during the period of about 50 μs (t_s) to 80 μs can be observed comparing Figs. 4 and 9, due to the fact that the DTT2 specimen can be bent further without the constraints from the supports and the tup.

Figure 10 shows the variations of the four energy quantities: input, kinetic, elastic and fracture. During $L_1 < t < L_2$, $L_3 < t < L_4$ and $t > L_5$, since the specimen loses contact with the tup, no increase in input energy occurs. It is noted from Fig. 10 that the total work done at $t = 180$ μs was about 53 J. This is less than half of the experimentally measured absorbed-energy value of 130 J. It should be noted that in the present "generation"-type study, since the energy balance calculations are "by-products" of the analysis, the energy quantities can be calculated very accurately.

3.3 DTT3 Specimen. The tup contact-force variation is shown in Fig. 11. Comparing Figs. 7 and 11, it is seen that during $L_1 < t < L_2$, the separation between the specimen and the tup, $(u_L - \bar{u}_L)$ is bigger than in the DTT2 case. This is attributed to the higher compliance of the DTT3 specimen due to the fact that growth initiation occurs much earlier. Also the second loss of contact of the specimen and the tup ($L_3 < t < L_4$) and second peak of P_L ($L_2 < t < L_3$) are smaller than those in the case of DTT2 specimen. Figure 12 shows the displacement of the specimen from the support point, and the support reaction force. Comparing Figs. 8 and 12, it is seen that the periods $S_1 - S_2$ and $S_2 - S_3$ are longer than those of the DTT2 specimen; and the peak value of P_s is smaller than that of DTT2. Again, these tendencies can be attributed to earlier crack initiation in this specimen.

Figure 13 shows the K-factor variation. Note that, as shown in Table 1, the crack growth initiation time was chosen to be $t = 35$ μs, such that $K_{Qd} = 65$ MNm$^{-1.5}$. In spite of this, the K-factor variation in DTT3 is more or less indentical to that in DTT2 (Fig. 11) until $t = 95$ μs. During the period of $t = 95$ μs to 146 μs, the K-value in DTT3 decreases while that of DTT2 increases. The variations of the four energy quantities are shown in Fig. 14. It is very interesting that during $V_1 < t < V_3$, a very small amount of energy is consumed in the fracture process.

3.4 DTT4 Specimen. The tup contact-force variation is shown in Fig 15. As seen from Fig. 2, the crack propagates faster in the DTT4 case than in the DTT2 case. Due to this

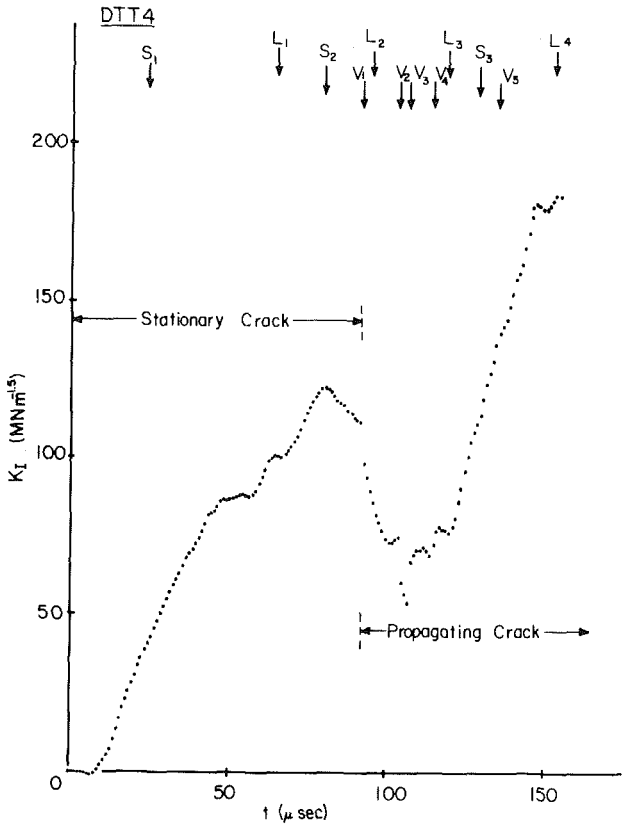

Fig. 17 Variation of dynamic stress intensity factor (DTT4)

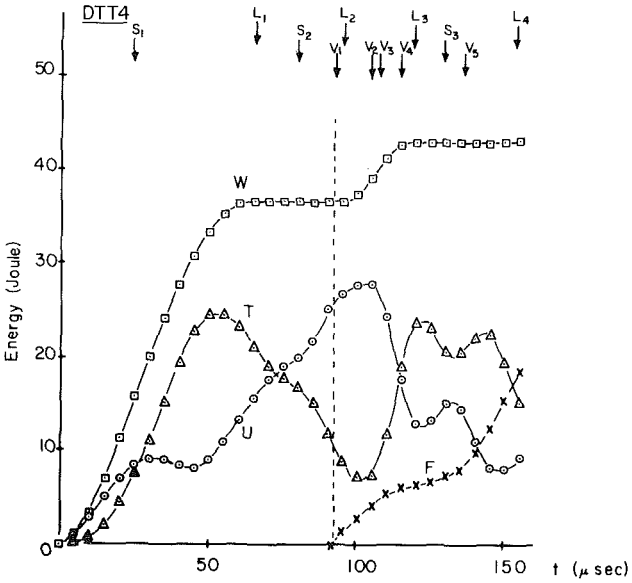

Fig. 18 Energy variations (DTT4)

reason, the changed compliances, the second peak of P_L ($L_2 < t < L_3$) is smaller and the second separation between the specimen and the tup, i.e., $(u_L - \bar{u}_L)$ between ($L_3 < t < L_4$), is larger in the DTT4 case than in the DTT2 case. The support reaction, and separation between supports and specimen are shown in Fig. 16. These are more or less similar to those in the DTT2 specimen.

From the K-factor variation shown in Fig. 17, it is seen that the K_{Qd} ($= K_{Id}$ in this case) value is about 111 MNm$^{-1.5}$. After initiation, the dynamic K-factor drops significantly. Prior to initiation, K_I value reaches the maximum value, 122

$MNm^{-1.5}$. It is noted that the analyses for the DTT2 and DTT4 are the same until the crack initiation in the DTT4 specimen ($t = 92.24$ μs). The energy variation plots are given in Fig. 18. In this case, the total energy to the specimen is lower than in the other three cases.

4 Discussion

The radius of the plane-strain plastic zone under the small-scale yielding condition, R_p, can be estimated by Irwin's simple approximation [10]

$$R_p = \frac{1}{6\pi}\left(\frac{K_I}{\sigma_{ys}}\right)^2 \tag{5}$$

where σ_{ys} is the yield stress of the material. The variation of estimated plastic zone size using equation (5), during the fracture process in the DTT specimens are shown in Fig. 19. Comparing R_p with the crack length a, ligament length $(W-a)$ and the specimen thickness, B, it can be seen from the figure that the estimated plastic zone sizes remain small until about 135.5 μs ~ 150 μs. After the crack length becomes $a/W = 0.7$, the plastic zone grows very rapidly, as seen in Fig. 19. Thus one can expect that the small-scale yielding condition is no longer satisfied after $a/W \geq 0.7$. However, until this point ($a/W < 0.7$), Fig. 19 seems to indicate the insignificant role of plasticity in the problem. Also, the inspection of fracture surfaces of the DTT specimen used in the experiment [1] reveal that the amount of plasticity accompanying crack growth was minimal in both the qausi-static and the impact tests.

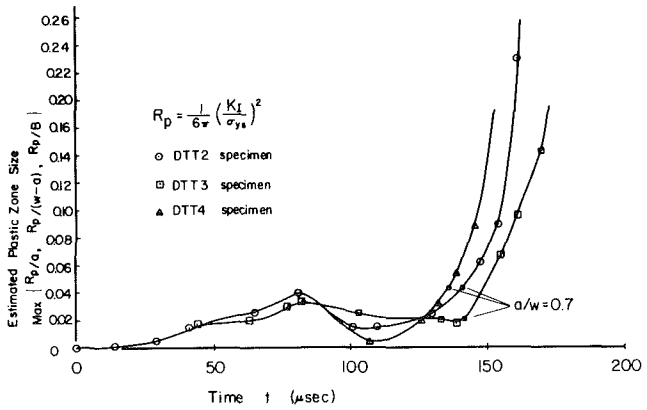

Fig. 19 Estimated plastic zone sizes around the crack tips during fracture in the DTT specimens

From the results obtained by the generation phase fracture simulation, in general, one can establish a unique relation between the dynamic fracture toughness for a propagating crack K_{ID} and the crack velocity v. In order to obtain an accurate and smooth K_{ID} versus v curve, the crack length history (and crack velocity history), which is the input data for the generation calculations, should be measured very accurately in the experiment, as done in reference [11]. Although rather poorly measured crack length histories (especially crack velocity histories), as seen in Fig. 2, were used as the input data in the present analyses, an attempt has been made to determine the K_{ID} versus v relation for this material.

Figure 20 shows the plot of K_I-values as function of the crack velocity v. Since we are investigating the dynamic fracture toughess under the regime of the small-scale yielding, the K_I-values for $a/W > 0.7$ were not plotted in Fig. 20. As seen from the figure, the present results are in favor of $K_{ID} = 65 + 0.044\ v$ $MNm^{-1.5}$, rather than $K_{ID} \approx 170$ $MNm^{-1.5}$. In fact, as seen form Figs. 9, 13, and 17, the K_I-values have never reached to 170 $MNm^{-1.5}$ until about 145 ~ 160 μs, at which the specimen ligaments became small, i.e., $(W-a)/W < 0.21 \sim 0.24$.

In the actual situation in the fracture specimens, the crack velocities vary steadily except immediately after initiation of crack propagation. The smoothness of K_I versus v curve depends strongly on the smoothness of crack velocity history used in the generation calculation. Thus, in the authors' opinion, at least a set of 15 to 20 data points for the crack velocity measurement should be required to obtain the accurate and smooth curve of K_{ID} versus v.

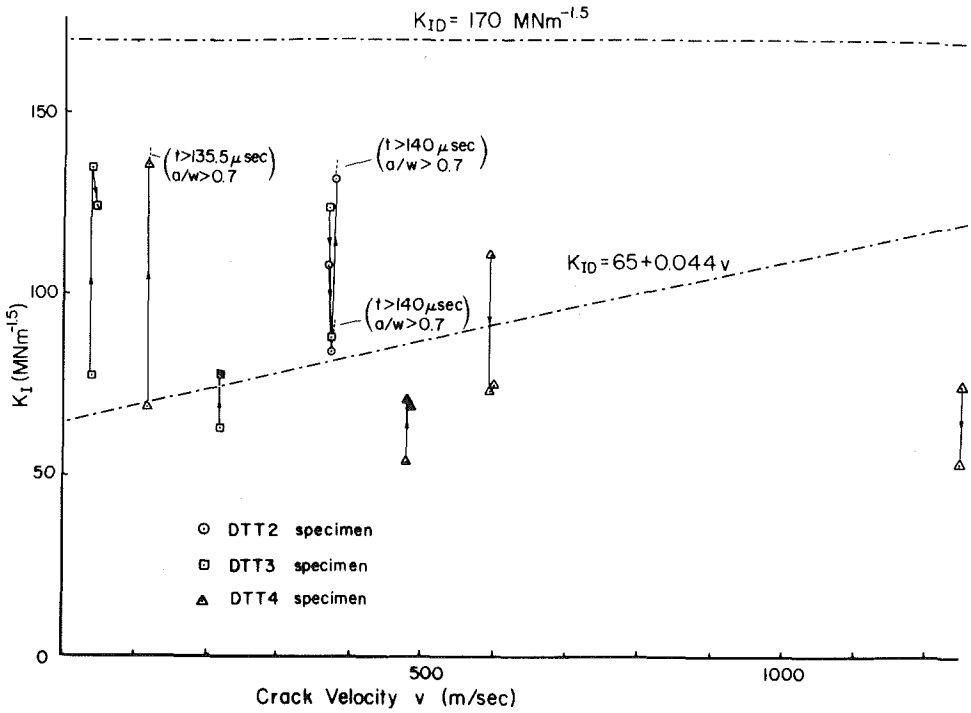

Fig. 20 Dynamic stress intensity factor as function of crack velocity

5 Conclusions

Utilizing the moving singularity element procedure, the generation phase simulations of fast fracture in the DTT specimen subject to impact loads have been performed for different crack propagtion histories and different boundary conditions at the tup and the support.

The major conclusions obtained from this study are summarized in the following:

1 The present results indicate that the initiation fracture toughness, K_{Qd} or K_{Id}, of about 108 $MNm^{-1.5}$ is related to the initiation time of about 95 μs, whereas the initiation fracture toughness of about 65 $MNm^{-1.5}$ is related to the intiation time of about 35 μs. Therefore, the determination of intiation fracture toughness depends strongly on the initiation time. In terms of the intiation stress intensity factor, no significant difference for a blunt notch (DTT2) and a sharp crack (DTT3) was observed.

2 Although the K_I versus v curve obtained by the present analyses is very rough due to the rough measurement of crack velocity in reference [1], the present K_I versus curve appears to support the equation $K_{ID} = 65 + 0.044\ v$ rather than $K_{ID} = 170\ MNm^{-1.5}$.

3 The stress intensity factors have never reached at the level of 170 $MNm^{-1.5}$ until the specimen ligaments became small, as long as the propagation histories provided in reference [1] were used.

4 Analyses with more realistic boundary conditions (contact/no-contact) at the tup and the supports give higher variations of stress intensity factors during the period of 50 to 80 μs. The effect of the separation of specimen from the tup or the supports propagates with the order of the shear wave velocity of the material.

Acknowledgments

This work was supported by the Office of Naval Research under Contract Number N00014-78-C-0636. The authors gratefully acknowledge this support. The encouragement of Dr. Y. Rajapakse is thankfully acknowledged. The authors express their appreciation to Ms. B. Bolinger for her help in preparing this manuscript.

References

1 Kanninen, M. F., Gehlen, P. C., Barnes, C. R., Hoagland, R. G., and Hahn, G. T., "Dynamic Crack Propagation Under Impact Loading," *Nonlinear & Dynamic Fracture Mechanics*, ASME Publication AMD-Vol. 35, eds., N. Perrone & S. N. Atluri, 1979, pp. 185-200.

2 Nishioka, T., and Atluri, S. N., "Numerical Modeling of Dynamic Crack Propagation in Finite Bodies, by Moving Singular Elements, Part I—Formulation," ASME *Journal of Applied Mechanics*, Vol. 47, 1980, pp. 570-577.

3 Nishioka, T., and Atluri, S. N., "Numerical Modeling of Dynamic Crack Propagation in Finite Bodies, by Moving Singular Elements, Part II—Results," ASME *Journal of Applied Mechanics*, Vol. 47, 1980, pp. 577-583.

4 Nishioka, T., and Atluri, S. N., "Numerical Analysis of Dynamic Crack Propagation: Generation and Prediction Studies," *Engineering Fracture Mechanics*, Vol. 16, No. 3, 1982, pp. 303-332.

5 Kanninen, M. F., private communication, Battelle's Columbus Labs, Jan. 1981.

6 Nishioka, T., and Atluri, S. N., "Finite Element Simulation of Fast Fracture in Steel DCB Specimen," *Engineering Fracture Mechanics*, Vol. 16, No. 2, 1982, pp. 157-175.

7 Mall, S., Kobayashi, A. S., and Urabe, Y., "Dynamic Photoelastic and Dynamic Finite Element Analysis of Polycarbonate Dynamic Tear Test Specimens," *Fracture Mechanics*, ASTM STP 677, ed., C. W. Smith, 1979, pp. 498-510.

8 Nishioka, T., Stonesifer, R. B., and Atluri, S. N., "An Evaluation of Several Moving Singularity Finite Element Procedures for Analysis of Fast Fracture," *Engineering Fracture Mechanics*, Vol. 15, No. 1-2, 1981, pp. 205-215.

9 Nishioka, T., and Atluri, S. N., "A Method for Determing Dynamic Stress Intensity Factors from COD Measurement at the Notch Mouth in Dynamic Tear Testing," *Engineering Fracture Mechanics*, Vol. 16, No. 3, 1982, pp. 333-339.

10 Irwin, G. R., "Comments on Dynamic Fracturing," *Fast Fracture and Crack Arrest*, ASTM STP 627, eds., G. T. Hahn and M. F. Kanninen, 1977, pp. 7-18.

11 Kalthoff, J. F., Beinert, J., and Winkler, S., "Measurements of Dynamic Stress Intensity Factors for Fast Running and Arresting Cracks in Double-Cantilever Beam Specimens," *Fast Fracture and Crack Arrest*, ASTM STP 627, eds., G. T. Hahn and M. F. Kanninen, 1977, pp. 161-176.